Applied Physics Letters

Experimental realization of phonon demultiplexing in three-dimensions

Cite as: Appl. Phys. Lett. **118**, 091901 (2021); https://doi.org/10.1063/5.0030830
Submitted: 24 September 2020 . Accepted: 11 February 2021 . Published Online: 02 March 2021

Osama R. Bilal, Chern Hwee Yee, Jan Rys, Christian Schumacher, and Chiara Daraio

Applied Physics Letters ARTICLE scitation.org/journal/apl

Experimental realization of phonon demultiplexing in three-dimensions

Cite as: Appl. Phys. Lett. **118**, 091901 (2021); doi: 10.1063/5.0030830
Submitted: 24 September 2020 · Accepted: 11 February 2021 ·
Published Online: 2 March 2021

Osama R. Bilal,[1,2,a)] Chern Hwee Yee,[2] Jan Rys,[2] Christian Schumacher,[3] and Chiara Daraio[4]

AFFILIATIONS

[1]Department of Mechanical Engineering, University of Connecticut, Storrs, Connecticut 06269, USA
[2]Department of Mechanical and Process Engineering, ETH Zürich, 8092 Zürich, Switzerland
[3]Computer Graphics Laboratory, ETH Zürich, 8092 Zürich, Switzerland
[4]Division of Engineering and Applied Science, California Institute of Technology, Pasadena, California 91125, USA

Note: This Paper is part of the APL Special Collection on Metastructures: From Physics to Applications.
[a)]**Author to whom correspondence should be addressed**: osama.bilal@uconn.edu

ABSTRACT

Phononic metamaterials enabled the realization of many acoustic components analogous to their electronic counterparts, such as transistors, logic gates, and calculators. A key component among these is the demultiplexer, a device that receives multiple signals and sorts them based on their frequencies into separate channels. Previous experimental realizations of acoustic and elastic multiplexers have employed plates with pillars or holes to demultiplex frequencies. However, existing realizations are confined to two dimensions, which can limit potential acoustic or elastic circuit design. Here, we show an experimental realization of a three-dimensional, four channel phononic demultiplexer. Our design methodology is based on bundles of pass-bands within a large bandgap that can easily be tuned for multi-channel frequency demultiplexing. The proposed design can be utilized in acoustic and elastic information processing, nondestructive evaluation, and communication applications, among others.

Phononic crystals and acoustic metamaterials consist of periodic arrangements of basic building blocks that repeat in space. These materials have the ability to control waves in an unprecedented manner, at different length and frequency scales. One of the unique properties of these materials is their ability to support forbidden frequency bands (i.e., bandgaps) in their dispersion spectrum. Within a bandgap, waves cannot propagate and are reflected toward the source. The main mechanisms for creating these forbidden bands within the frequency spectrum are either destructive interference (e.g., in Bragg scattering bandgaps) or local resonance. When a bandgap is open due to Bragg scattering, the wavelength of the affected waves is usually at the same order of the spacing between the unit cells (i.e., lattice spatial periodicity).[1,2] In contrast, when a bandgap is open due to resonances, the wavelength of the attenuated waves can be independent of the lattice spacing.[3] Such resonances induce properties that might not exist in conventional materials, like negative effective mass or stiffness.[4–6] Phononic crystals and metamaterials with such exotic properties have been utilized for many applications such as vibration and sound insulation,[7,8] seismic wave protection,[9,10] wave guiding,[11,12] and frequency filtering,[13,14] among others.[15]

Phononic crystals and metamaterials have been proposed as platforms to enable mechanical information processing. Potential applications range from thermal computing[16–18] (at small scales) to ultrasound and acoustic based computing (at larger scales).[19,20] Current realizations of fundamental phonon computing elements such as acoustic switches,[21,22] rectifiers,[23,24] diodes,[25–28] transistors,[29,30] memory,[31] and lasers[32,33] have been inspired by their electronic counterparts. Among such devices, demultiplexers are combinational logic devices that take a single input at one end and route it to one of the several output channels [Fig. 1(a)]. There exist multiple theoretical proposals for realizing phonon demultiplexers for both acoustic[13,34,35] and elastic waves[36–46] with few experimental demonstrations.[35,47,48] The main working principle for most of these designs is based on embedded cylinders,[13,36,46,49] holes,[47] or pillars[48] in a host plate. These realizations constrain demultiplexing phonons to two dimensions. A device that can demultiplex phonons in three dimensions for all wave polarization remains elusive. In this paper, we numerically design and experimentally characterize a 3D phonon demultiplexer for elastic waves [Fig. 1(b)].

To realize our demultiplexer, we design a cubic unit cell that has two important characteristics: (1) a wide bandgap to filter out

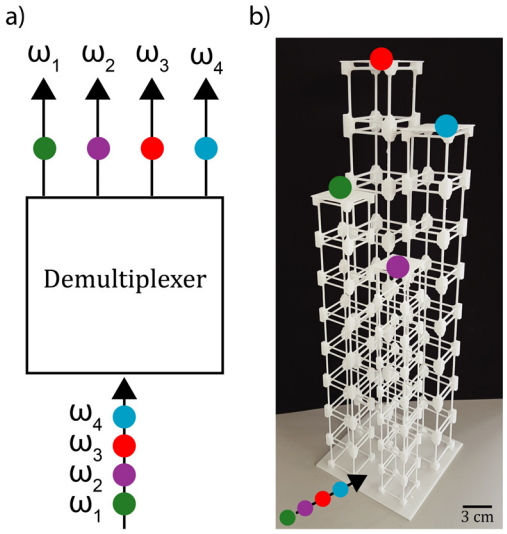

FIG. 1. 3D Phononic demultiplexer. (a) A conceptual schematic of a 4-channel demultiplexer with four different input frequencies excited at one end and sorted in four predefined channels at the other end. (b) A 3D-printed realization of the 4-channel phonon demultiplexer, where four different frequencies are excited at the base and passively sorted into their corresponding channel.

undesirable frequencies and (2) a bundle of pass bands inside the large bandgap to allow only the targeted frequencies to pass. The unit cell is composed of eight masses, one at each of the unit cell's corners, connected by 12 beams [Fig. 2(a)].

To verify our design hypothesis, we first consider an infinite unit cell model, where one single unit cell is assumed to repeat in space in all directions. We analyze the unit cell using Bloch periodic boundary conditions.[50] The dispersion curves of the unit cell, correlating wavenumber with frequency, are calculated using the wave equations for heterogeneous media[51] within an infinite medium. We use the finite element method to solve the elastic wave equations (COMSOL 5.4). The solution is the wavefunction $u(x,\kappa;t) = \tilde{u}(x)\exp^{(i(\kappa^\top x-\omega t))}$, where $\tilde{u}$ is the Bloch displacement vector, x is the position vector, κ is the wavenumber, ω is the frequency, and t is the time. The resulting dispersion curves are normalized by the unit cell size and the longitudinal speed of sound in the medium, $\Omega = fa/c$. The dispersion nondimensionalization comes at no loss of generality as it is first calculated with all the considered material parameters. The dispersion plot shows a significant bandgap [shaded gray region in Fig. 2(b)] with a relative width of ≈124%. The relative width of the bandgap is calculated as the absolute width of the bandgap divided by its central frequency. Within the bandgap region, there exist two pass bands with a central frequency of $\Omega = 0.29$ and 0.53, which we engineer to work as the transmission bands for our demultiplexer.

To better explain the behavior of the proposed design, we visualize the unit cell's vibrational mode shapes by superimposing the displacement profiles as a heat map over its geometry for eight different frequencies [Fig. 2(c)]. The first two mode shapes ($\Omega_{1,2} = 0.08$ and 0.1) resemble the first vibrational modes of the beams connecting the corner masses. The third and fourth modes ($\Omega_{3,4} = 0.15$ and 0.17) show the mixed resonance modes of the corner masses along with the first vibrational modes of the connecting beams. All four modes exist below the

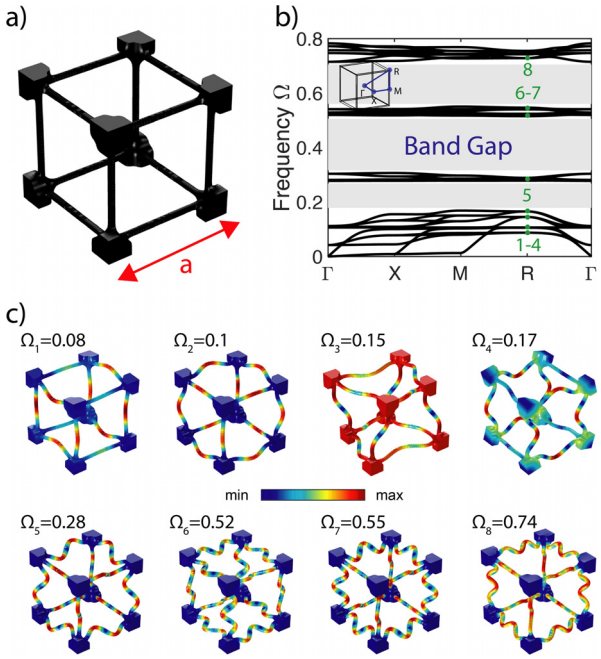

FIG. 2. Basic building block. (a) The unit cell composed of eight masses at its corners connected with 12 beams forming a cube. (b) Dispersion curves of the metamaterial unit cell along the path $\Gamma - X - M - R - \Gamma$ assuming infinite repetition of the unit cell in all directions. Full bandgaps, where waves are prohibited from propagation, are highlighted in gray. The inset shows the irreducible Brillouin zone for a symmetric cubic unit cell. (c) Selected elastic mode shapes of the unit cell at the *R* point at the four different transmission bands.

bandgap. The fifth mode shape, which exists in the first passband ($\Omega_5 = 0.28$), shows the second vibrational mode of the connecting beams. The third vibrational mode of the unit cell beams manifests itself within the second passband ($\Omega_{6,7} = 0.52$ and 0.55). At the edge of the bandgap ($\Omega_8 = 0.74$), the connecting beams vibrate in their fourth mode shape. The masses work as pivots or fixation points for the connecting slender beams, which behave as fixed-fixed beams with well-defined vibrational mode shapes. We note the existence of a very low frequency branch(es) along the path $\Gamma - X$ and $X - M$, due to the lack of the diagonal coupling between the corner masses. In addition, the simple geometry of the unit cell causes many of the vibrational mode shapes to be degenerate. Based on this simple design concept, the unit cell can be considered as a simple mass spring model with a large bandgap with embedded bands of transmission. By changing the diameter of the beams or the ratio between the mass of the beam and the mass of the corner block, we can change the position of the bandgap and its width. Alternatively, by scaling the unit cell length a, we can shift the position of the bandgap along with its embedded pass bands within the frequency spectrum. An advantage of scaling the entire unit cell, while keeping all aspect ratios the same, is preserving all the dispersion characteristics of the unit cell (e.g., group velocities) without alteration. This preservation can help in maintaining consistency in the performance of the different channels, such as the mode shapes and wave polarization.

The demultiplexer is constructed by designing four channels out of the *same* unit cell, but with four different lattice constants. All four

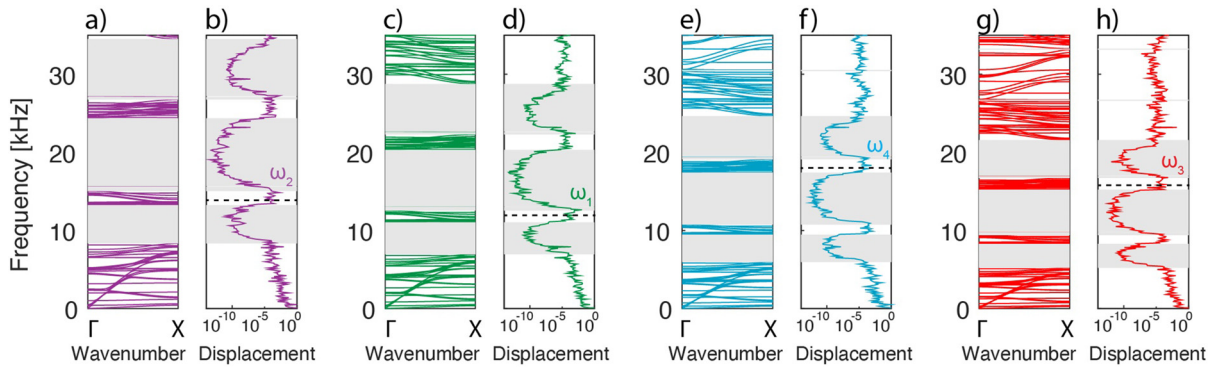

FIG. 3. Infinite medium vs finite structure. The calculated dispersion curves and their corresponding frequency response functions (FRFs) for unit cells with the side length equal to (a) and (b) 30 mm, (c) and (d) 36 mm, (e) and (f) 42 mm, and (g) and (h) 48 mm. The dispersion curves are calculated along the $\Gamma - X$ direction with periodicity only along the x direction. The FRFs are calculated for a structure composed of $1 \times 1 \times 8$ unit cells. The bandgaps are highlighted in gray in both dispersion curves and FRFs. The dashed horizontal lines mark the operational frequencies used in the different channels.

channels are connected at one end (i.e., the base of the demultiplexer). The excitation takes place at the base with multiple frequencies that get sorted into the four channels. To correctly confirm the behavior of the scaled unit cells, we calculate the dispersion curves for four different lattice constants $a = 30$, 36, 42, and 48 mm [Figs. 3(a), 3(c), 3(e), and 3(g)]. The dispersion curves for these four unit cells are calculated based on 1D Bloch periodicity (only along the κ_x direction). Basing the analysis on 1D periodicity, as opposed to 3D periodicity, gives rise to extra modes along the free boundaries with no periodicity. These boundary modes manifest themselves as added lines in the dispersion curves. A clear difference between the 1D and 3D periodic dispersion curves can be seen, for example, by comparing the number of branches below the first bandgap in Figs. 2(b) and 3(a). A detailed comparison between 1D, 2D, and 3D periodicity is presented in the supplementary material. The existence of multiple flat or quasi-flat lines is mainly due to the added standing modes and does not affect the transmission signal. This can be seen in the amplitude of the transmission within the narrow pass bands in comparison to the transmission in the large pass bands at higher frequencies [Figs. 3(b), 3(d), 3(f), and 3(h)]. The 1D periodic dispersion curves serve as the limiting case for the performance of the proposed design. As more periodicity is incorporated in the model (i.e., along κ_y and κ_z directions), less vibration modes become available at the free boundaries and the dispersion curves become identical to Fig. 2(b). Therefore, having a demultiplexer channel with more unit cells in all directions will result in less dispersion lines and wider band gaps. A variation in the presented design with input signals from all directions is presented in the supplementary material.

To validate the infinite unit cell model against the finite structure with all the connected channels, we numerically simulate the exact geometry of the demultiplexer as seen in Fig. 1(b) using the finite element method. Each channel is composed of an array of 8 unit cells tessellated along the z direction. All channels are connected to a baseplate with a thickness of $T_h = 3$ mm. The top end of each channel is terminated by a plate with the same thickness for signal extraction. The plate thickness, T_h, is chosen such that its resonance frequencies (i.e., the plate mode shapes) do not coincide with the operational frequencies of the channels. The channels are arranged in a 2×2 grid separated by 30 mm. A harmonic excitation is applied at the bottom surface of the baseplate. We sweep the excitation frequency between 1 and 32 kHz and record the displacement at the end of each of the channels [Figs. 3(b), 3(d), 3(f), and 3(h)]. The predicted bandgap frequencies using the infinite unit cell model are shaded in gray in all panels of Fig. 3. The results of both the finite and infinite models are in very good agreement. Within the band gaps, shown as the gray shaded regions in Fig. 3, the amplitude of the transmitted wave is many orders of magnitude less than that of the passband frequencies. The fact that all channels are connected at the base does not affect the robustness of the individual channels' performance. In addition, we also plot the logarithm of the full displacement fields as a heat map at the four operational frequencies of the demultiplexer (Fig. 4). The displacement field at each frequency shows a clear transmission of elastic phonons at targeted frequency, while the rest of the channels show negligible motion.

To experimentally validate our numerical simulations, we fabricate the demultiplexer through additive manufacturing (laser sintering) using polyamide (Young's modulus $E = 2.3$ GPa and density

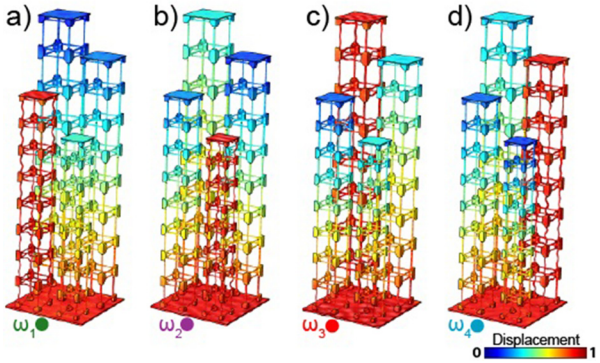

FIG. 4. Demultiplexer numerical simulations. Numerically calculated mode shapes of the demultiplexer operating at (a) $\omega_1 = 11.7$ kHz, (b) $\omega_2 = 13.9$ kHz, (c) $\omega_3 = 15.9$ kHz, and (d) $\omega_4 = 18.1$ kHz. The heat map represents the normalized intensity of motion (i.e., the logarithm of displacement divided by its maximum amplitude) through the entire structure when excited at the base.

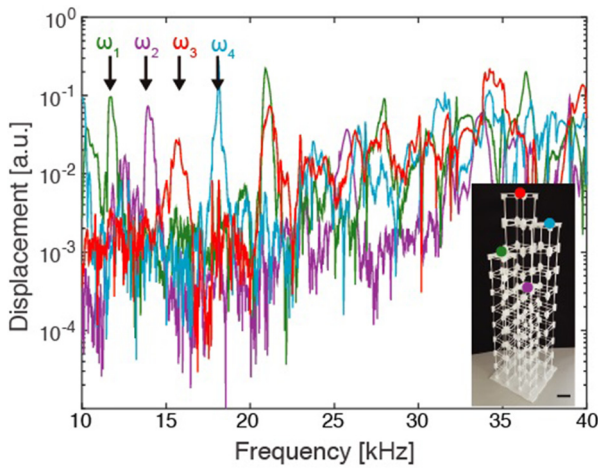

FIG. 5. Demultiplexer experimental characterization. Experimental measurements of the displacement at the end of each channel as a function of frequency. The targeted frequencies are marked with black arrows with $\omega_1 = 11.7$ kHz, $\omega_2 = 13.9$ kHz, $\omega_3 = 15.9$ kHz, and $\omega_4 = 18.1$ kHz. The scale bar is 3 cm in the inset.

$\rho = 1200\,\mathrm{Kg/m^3}$). We characterize the vibration response of the meta-device by harmonically exciting the baseplate with a piezoelectric disk (repeating the previously performed numerical simulations in Figs. 3 and 4). We measure the transmitted vibrations at the end of each channel using a laser Doppler vibrometer LDV (Polytec OFV-505 with an OFV-5000 decoder, using a VD-06 decoder card). We excite the system by sweeping through frequencies between 10 and 40 kHz and record the amplitude of the transmitted vibrations at the end of each channel (Fig. 5). In general, the measured signals at the end of each channel are in very good agreement with the numerical simulations. In particular, the size and position of the bandgaps seem to support our numerical predictions. More importantly, the measured vibrations between 10 and 20 kHz show a clear bandgap, as predicted by the numerical simulations in all channels, and demonstrate clear transmission of the signal in the designated pass bands in each channel. The experimental measurements show clear evidence of phonon demultiplexing based on frequency in the realized meta-device.

In this study, we design, analyze, and realize the first 3D phononic demultiplexer. Our design relies on defining relatively narrow pass bands within a wide bandgap. Designing the width of the pass-band allows for a wider operational bandwidth and ensures transmission of each signal to its designated channel. The complete bandgap for all directions and polarization (in-plane, out of plane, and rotation) of the wave allows for phonon demultiplexing in three dimensions. Multiplexing elastic and acoustic waves in 3D can enable the design of higher dimensional all-phononic circuits, taking advantage of the recent progress in advanced manufacturing. Due to these advances in fabrication and the material invariant nature of the design principle, our meta-device can be easily scaled to operate at desired frequencies with no geometry alteration. For example, the same design fabricated at half the size would operate around twice the frequency (i.e., in the ultrasound regime). Our demultiplexer has possible applications in imaging, communications, and phonon-based information processing.

See the supplementary material for detailed dispersion curves with different periodic boundary conditions and an alternative design of the multiplexer based on our unit cell.

The authors are very grateful for the fruitful discussions with Dr. Foehr and his help with the experimental setup. C. D. acknowledges support from the National Science Foundation under EFRI Grant No. 1741565. O. R. B. acknowledges support from the University of Connecticut start-up funds.

DATA AVAILABILITY

All the data supporting the findings in this study are available in this article and its supporting information. Further data and methods are available from the corresponding author upon reasonable request.

REFERENCES

[1]M. Kushwaha, P. Halevi, L. Dobrzynski, and B. Djafari-Rouhani, "Acoustic band structure of periodic elastic composites," Phys. Rev. Lett. **71**, 2022–2025 (1993).
[2]M. Sigalas and E. Economou, "Band structure of elastic waves in two dimensional systems," Solid State Commun. **86**, 141–143 (1993).
[3]Z. Liu, X. Zhang, Y. Mao, Y. Zhu, Z. Yang, C. Chan, and P. Sheng, "Locally resonant sonic materials," Science **289**, 1734–1736 (2000).
[4]J. Christensen, M. Kadic, O. Kraft, and M. Wegener, "Vibrant times for mechanical metamaterials," MRS Commun. **5**, 453–462 (2015).
[5]S. A. Cummer, J. Christensen, and A. Alù, "Controlling sound with acoustic metamaterials," Nat. Rev. Mater. **1**, 16001 (2016).
[6]G. Ma and P. Sheng, "Acoustic metamaterials: From local resonances to broad horizons," Sci. Adv. **2**, e1501595 (2016).
[7]Z. Yang, H. Dai, N. Chan, G. Ma, and P. Sheng, "Acoustic metamaterial panels for sound attenuation in the 50–1000 Hz regime," Appl. Phys. Lett. **96**, 041906 (2010).
[8]O. R. Bilal, D. Ballagi, and C. Daraio, "Architected lattices for simultaneous broadband attenuation of airborne sound and mechanical vibrations in all directions," Phys. Rev. Appl. **10**, 054060 (2018).
[9]S.-H. Kim and M. P. Das, "Seismic waveguide of metamaterials," Mod. Phys. Lett. B **26**, 1250105 (2012).
[10]S. Brûlé, E. Javelaud, S. Enoch, and S. Guenneau, "Experiments on seismic metamaterials: Molding surface waves," Phys. Rev. Lett. **112**, 133901 (2014).
[11]M. Torres, F. Montero de Espinosa, D. Garcia-Pablos, and N. Garcia, "Sonic bandgaps in finite elastic media: Surface states and localization phenomena in linear and point defects," Phys. Rev. Lett. **82**, 3054–3057 (1999).
[12]C. J. Rupp, A. Evgrafov, K. Maute, and M. L. Dunn, "Design of phononic materials/structures for surface wave devices using topology optimization," Struct. Multidiscip. Optim. **34**, 111–121 (2007).
[13]Y. Pennec, B. Djafari-Rouhani, J. Vasseur, A. Khelif, and P. A. Deymier, "Tunable filtering and demultiplexing in phononic crystals with hollow cylinders," Phys. Rev. E **69**, 046608 (2004).
[14]C. J. Rupp, M. L. Dunn, and K. Maute, "Switchable phononic wave filtering, guiding, harvesting, and actuating in polarization-patterned piezoelectric solids," Appl. Phys. Lett. **96**, 111902 (2010).
[15]M. Maldovan, "Sound and heat revolutions in phononics," Nature **503**, 209–217 (2013).
[16]B. Li, L. Wang, and G. Casati, "Negative differential thermal resistance and thermal transistor," Appl. Phys. Lett. **88**, 143501 (2006).
[17]L. Wang and B. Li, "Thermal logic gates: Computation with phonons," Phys. Rev. Lett. **99**, 177208 (2007).
[18]K. Joulain, J. Drevillon, Y. Ezzahri, and J. Ordonez-Miranda, "Quantum thermal transistor," Phys. Rev. Lett. **116**, 200601 (2016).
[19]S. Bringuier, N. Swinteck, J. Vasseur, J.-F. Robillard, K. Runge, K. Muralidharan, and P. Deymier, "Phase-controlling phononic crystals: Realization of acoustic Boolean logic gates," J. Acoust. Soc. Am. **130**, 1919–1925 (2011).
[20]T. Zhang, Y. Cheng, J.-Z. Guo, J.-Y. Xu, and X.-J. Liu, "Acoustic logic gates and boolean operation based on self-collimating acoustic beams," Appl. Phys. Lett. **106**, 113503 (2015).

[21]S. Babaee, N. Viard, P. Wang, N. X. Fang, and K. Bertoldi, "Harnessing deformation to switch on and off the propagation of sound," Adv. Mater. **28**, 1631 (2016).
[22]O. R. Bilal, A. Foehr, and C. Daraio, "Reprogrammable phononic metasurfaces," Adv. Mater. **29**, 1700628 (2017).
[23]B. Liang, B. Yuan, and J-c Cheng, "Acoustic diode: Rectification of acoustic energy flux in one-dimensional systems," Phys. Rev. Lett. **103**, 104301 (2009).
[24]B. Liang, X. Guo, J. Tu, D. Zhang, and J. Cheng, "An acoustic rectifier," Nat. Mater. **9**, 989–992 (2010).
[25]B.-I. Popa and S. A. Cummer, "Non-reciprocal and highly nonlinear active acoustic metamaterials," Nat. Commun. **5**, 3398 (2014).
[26]X.-F. Li, X. Ni, L. Feng, M.-H. Lu, C. He, and Y.-F. Chen, "Tunable unidirectional sound propagation through a sonic-crystal-based acoustic diode," Phys. Rev. Lett. **106**, 084301 (2011).
[27]T. Devaux, V. Tournat, O. Richoux, and V. Pagneux, "Asymmetric acoustic propagation of wave packets via the self-demodulation effect," Phys. Rev. Lett. **115**, 234301 (2015).
[28]N. Boechler, G. Theocharis, and C. Daraio, "Bifurcation-based acoustic switching and rectification," Nat. Mater. **10**, 665–668 (2011).
[29]D. Hatanaka, I. Mahboob, K. Onomitsu, and H. Yamaguchi, "A phonon transistor in an electromechanical resonator array," Appl. Phys. Lett. **102**, 213102 (2013).
[30]O. R. Bilal, A. Foehr, and C. Daraio, "Bistable metamaterial for switching and cascading elastic vibrations," Proc. Natl. Acad. Sci. U. S. A. **114**, 4603–4606 (2017).
[31]D. Hatanaka, I. Mahboob, K. Onomitsu, and H. Yamaguchi, "Mechanical random access memory in a phonon circuit," Appl. Phys. Express **7**, 125201 (2014).
[32]K. Vahala, M. Herrmann, S. Knünz, V. Batteiger, G. Saathoff, T. Hänsch, and T. Udem, "A phonon laser," Nat. Phys. **5**, 682–686 (2009).
[33]H. Jing, S. Özdemir, X.-Y. Lü, J. Zhang, L. Yang, and F. Nori, "PT-symmetric phonon laser," Phys. Rev. Lett. **113**, 053604 (2014).
[34]B. Rostami-Dogolsara, M. K. Moravvej-Farshi, and F. Nazari, "Designing switchable phononic crystal-based acoustic demultiplexer," IEEE Trans. Ultrason., Ferroelectr., Freq. Control **63**, 1468–1473 (2016).
[35]A. A. Watkins and O. R. Bilal, "Demultiplexing infrasound phonons with tunable magnetic lattices," Front. Mater. **7**, 410 (2020).
[36]Q. Zou, W. Liu, T. Yu, N. Liu, T. Wang, and Q. Liao, "Decoupling of multiple coupled phononic crystal waveguides: Application to acoustic demultiplexing," J. Phys. D: Appl. Phys. **50**, 125102 (2017).
[37]P. Moradi and A. Bahrami, "Three channel ghz-ranged demultiplexer in solid-solid phononic crystals," Chin. J. Phys. **59**, 291–297 (2019).
[38]F. Motaei and A. Bahrami, "Eight-channel acoustic demultiplexer based on solid-fluid phononic crystals with hollow cylinders," Photonics Nanostruct.-Fundam. Appl. **39**, 100765 (2020).
[39]F. Nazari and J. Babaki, "Heterostructure based demultiplexer using solid-solid phononic crystal ring resonators," J. Phys. D: Appl. Phys. **50**, 375301 (2020).
[40]Y. Ben-Ali, A. Khaled, and D. Bria, "Y-Shaped branch structure using asymmetric resonators for phononic demultiplexing," Mater. Today **27**(4), 3033–3041 (2020).
[41]H. Gharibi and A. Bahrami, "Phononic crystals for sensing fames with demultiplexed frequencies," J. Mol. Liq. **305**, 112841 (2020).
[42]Y. Pennec, B. Djafari-Rouhani, J. Vasseur, H. Larabi, A. Khelif, A. Choujaa, S. Benchabane, and V. Laude, "Channel drop process of elastic wave in a two dimensional phononic crystal," in *IEEE Ultrasonics Symposium* (IEEE, 2005), Vol. 1, pp. 69–72.
[43]M. I. Hussein, G. M. Hulbert, and R. A. Scott, "Hierarchical design of phononic materials and structures," in International Mechanical Engineering Congress and Exposition (IMECE) (2005), Vol. 42258, pp. 163–172.
[44]Y. Jin, Y. Pennec, Y. Pan, and B. Djafari-Rouhani, "Phononic crystal plate with hollow pillars connected by thin bars," J. Phys. D: Appl. Phys. **50**, 035301 (2017).
[45]Y. Jin, N. Fernez, Y. Pennec, B. Bonello, R. P. Moiseyenko, S. Hémon, Y. Pan, and B. Djafari-Rouhani, "Tunable waveguide and cavity in a phononic crystal plate by controlling whispering-gallery modes in hollow pillars," Phys. Rev. B **93**, 054109 (2016).
[46]J. Vasseur, O. B. Matar, J. Robillard, A.-C. Hladky-Hennion, and P. A. Deymier, "Band structures tunability of bulk 2D phononic crystals made of magneto-elastic materials," AIP Adv. **1**, 041904 (2011).
[47]S. Mohammadi and A. Adibi, "On chip complex signal processing devices using coupled phononic crystal slab resonators and waveguides," AIP Adv. **1**, 041903 (2011).
[48]M. S. Faiz, M. Addouche, A. R. M. Zain, K. S. Siow, A. Chaalane, and A. Khelif, "Experimental demonstration of a multichannel elastic wave filter in a phononic crystal slab," Appl. Sci. **10**, 4594 (2020).
[49]B. Rostami-Dogolsara, M. K. Moravvej-Farshi, and F. Nazari, "Acoustic add-drop filters based on phononic crystal ring resonators," Phys. Rev. B **93**, 014304 (2016).
[50]F. Bloch, "U about the quantum mechanics of electrons in crystal lattices," J. Phys. **52**, 555–600 (1929).
[51]K. F. Graff, *Wave Motion in Elastic Solids* (Courier Corporation, 2012).